Coherent population trapping for reservoir engineering and spin squeezing

Anying Feng, Jun Xu,* and Xiangming Hu†
College of Physical Science and Technology, Central China Normal University, Wuhan 430079, People's Republic of China

(Received 1 February 2024; accepted 16 August 2024; published 6 September 2024)

Spin squeezing has important applications in the field of quantum metrology and quantum information processing. Here we propose that coherent population trapping is well suitable for establishing cavity dissipation mechanism and generating a spin-squeezed state. An ensemble of N double Λ-type atoms is placed inside the two-mode optical cavity, where one Λ subsystem is driven resonantly by two strong control fields to form a dark resonance and the other Λ subsystem is coupled by two cavity vacuum fields and two external fields with large detunings. Due to the dark resonance, the atoms are trapped in a dark state and one has the maximal coherence between the two ground states. Two double off-resonance stimulated Raman scattering interactions are induced between fields and dressed atoms to establish a dissipative quantum dynamical process based on a collective cavity reservoir. As a result, strong stable spin squeezing is generated, which is verified by our numerical and analytical results.

DOI: 10.1103/PhysRevResearch.6.033256

I. INTRODUCTION

In the field of quantum metrology, the measurement precision with uncorrelated particles is restricted by the standard quantum limit (SQL), which arises from the quantum noise inherent in measurements [1]. However, this limit can be overcome by exploiting quantum correlated states, such as spin-squeezed states (SSSs) [2–6]. These states are entangled quantum states of collective spins with reduced quantum fluctuations in one spin component perpendicular to the mean spin direction by increasing the fluctuations of the other component [7,8]. The reduced quantum fluctuations can improve the measurement precision, even up to the Heisenberg limit (HL). The SSSs have many important applications in the improvement of high-precision measurements, e.g., Ramsey spectroscopy [9–20], atomic clocks [21–31], magnetometers [32–43], and gravitational-wave interferometers [44–50].

Up to now, there are many methods for preparing SSSs, which can be roughly divided into the following three categories. One method is to transfer the squeezing states of light to the spin system directly [51–56]. It is determined by the quality of squeezed light and the transfer efficiency. Another method is to perform the quantum nondemolition measurement on the states of photons coupled with the atomic ensemble [4,5,57–63]. The generating spin squeezing is nondeterministic and depends entirely on the results of the measurement. In fact, the spin squeezing is greatly affected by the spontaneous radiation of atomic ensemble itself and the detection efficiency of photon detector. The last method is based on the nonlinear atom-atom interaction. Compared to the first two methods, the acquired spin-squeezed state can be generated deterministically with no need for high-quality squeezing lights and efficient quantum detectors. There are many theoretical proposals for implementing such nonlinear interactions, some of which have been implemented experimentally, such as in Bose-Einstein condensates via atomic collisions [3,64–68], in atomic ensembles via photon-induced atom-atom interactions [69–84], and in diamond nanostructures via phonon-induced spin-spin interactions [85–89].

Among the category of nonlinear atom-atom interaction platforms, Sørensen and Mølmer used double off-resonance stimulated Raman scattering (SRS) to realize one-axis twisting (OAT) [70]. This method can also been extended to two-axis twisting (TAT) via adding another two classical driving fields [71]. Until now, a number of schemes based on the SRS processes have been put forward to generate the SSSs. For example, Torre *et al.* excited a pair of two-photon Raman transitions in a four-level atomic ensemble and constructed a collective atomic dark state to feature spin squeezing [73]. In this similar configuration, Zhang *et al.* realized the two-axis countertwisting spin-squeezing Hamiltonian with the aid of phase-locked atom-photon coupling [74]. Recently, Liu *et al.* implemented a single off-resonance SRS in a three-level atomic ensemble to produce OAT and TAT spin squeezing [77]. The SRS process requires a large detuning between the atom ensemble and the field to ensure their dispersive interaction. In the large detuning regimes, the atoms are hardly excited and spontaneous emission is almost avoided. However, there are two disadvantages for those approaches based on the SRS process between the bare states. One is that the atoms stay dominantly in a single bare state and have only small coherence or zero average coherence between two ground states. Generally speaking, quantum information processing requires large quantum coherent nodes. The other is that the strengths of the spin interaction are relatively small. Once the strengths are not enough to overcome the

*Contact author: junxu@ccnu.edu.cn
†Contact author: xmhu@ccnu.edu.cn

decoherence noises, the possible spin squeezing will be washed out.

In this paper, we propose a scheme based on the cavity dissipation mechanism to generate the steady spin-squeezed state in CPT. We consider an atomic ensemble with a double Λ-type configuration, where one Λ subsystem is driven resonantly by two strong control fields to form a dark resonance and the other Λ subsystem is coupled by two cavity vacuum fields and two external fields with the large detunings. It is well-known that CPT is one of the most remarkable resonant coherent effects. The dark resonance means that the atoms are trapped in a superposition of two ground states, no longer excited, and there is the maximal coherence between the two ground states. The dispersion interactions between the two cavity fields, the two external fields, and the dressed atoms induce two double off-resonance SRS interactions between the atomic dressed states. A dissipative quantum dynamical process is established based on a collective cavity reservoir. In this case, the cavity dissipation play an positive role for the generation of the steady spin-squeezed state. Comparing to previous schemes, our scheme has the following striking features: (i) Due to the dark resonance, the atoms are hardly excited but oscillate between two long-lived ground states and the maximal coherence exists between the two ground states. The SRS interactions are induced between the fields and the atomic dressed states, but not the bare states. (ii) This dissipation mechanism is robust against the environmental noise and does not need the initial preparation of the nonclassical states. (iii) The obtained spin-squeezed state is stable and deterministic with no need for efficient quantum detectors.

The remaining part of this paper is organized as follows. In Sec. II, we describe the system model and master equation. In Sec. III, we give the cavity-spin interaction based on CPT. In Sec. IV, we discuss the spin squeezing induced by dissipation and give the numerical results of the general case, the analytical description of the special case, and the experimental implementations. Finally, a conclusion is given in Sec. V.

II. MODEL AND MASTER EQUATION

We first describe our system and present the master equation. As sketched in Fig. 1, an ensemble of N double Λ-type atoms is placed inside the two-mode optical cavity. The atomic ensemble is driven by two strong control fields with Rabi frequencies $\Omega_{1,2}$ and two external fields with Rabi frequencies $\varepsilon_{1,2}$. The two control fields $\Omega_{1,2}$ are applied to drive the atomic electronic dipole-allowed transitions $|1,2\rangle \leftrightarrow |3\rangle$ resonantly. The two cavity fields $a_{1,2}$ and the two external fields $\varepsilon_{1,2}$ are coupled to the atomic electronic dipole-allowed transitions $|1,2\rangle \leftrightarrow |4\rangle$ with the large detunings. $|1\rangle \leftrightarrow |2\rangle$ is electronic-dipole forbidden. The Heisenberg-Langevin equation for the operator o of the atom-field system is written as

$$\dot{o} = -\Gamma_o o + \frac{i}{\hbar}[H, o] + F_o(t), \tag{1}$$

where the operator o includes the atomic operators $\sigma_{jk}(j,k = 1,2,3,4)$ and the field operators $a_l, a_l^\dagger (l = 1,2)$. Here $\sigma_{jk} = \sum_{\mu=1}^{N} |j^\mu\rangle\langle k^\mu|$ are the collective projection operators for $j = k$ and the collective spin-flip operators for $j \neq k$. a_l and $a_l^\dagger$ denote the annihilation and creation operators of the cavity modes. The spontaneous emission rates of the atoms from the excited states $|3\rangle(|4\rangle)$ to the ground states $|l\rangle$ are represented by $\gamma_{3l}(\gamma_{4l})$, the dephasing rate between the two ground states is represented by γ_p, and the cavity loss rates are represented by κ_l. The dissipation term Γ_o is determined by these decay rates and satisfies the relation $\Gamma_o = \Gamma_{o^\dagger}$, which is given in Appendix A. $F_o(t)$ is the noise force with zero average and shows a δ correlation with an associated diffusion coefficient that can be found using Einstein relation. The total Hamiltonian of the system reads

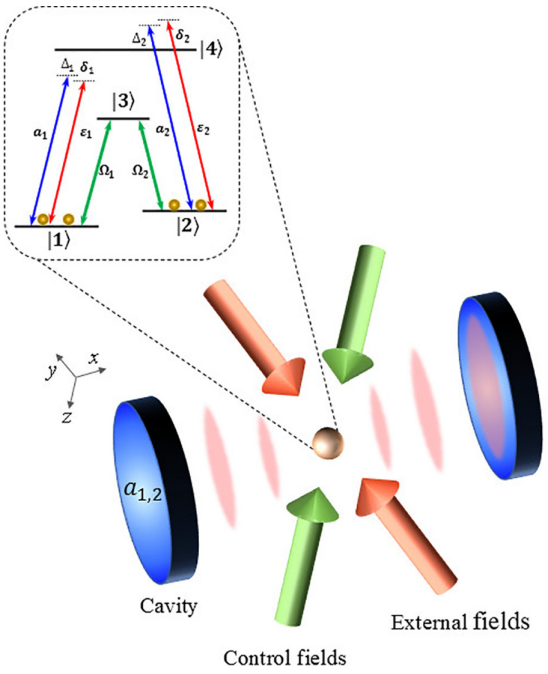

FIG. 1. Sketch of the proposed scheme. An ensemble of N double Λ-type atoms with two ground states $|1,2\rangle$ and two excited states $|3,4\rangle$ is placed inside the two-mode optical cavity along the x direction. The atomic ensemble is driven by two strong control fields with Rabi frequencies $\Omega_{1,2}$ along the z direction, and simultaneously interacts with two external fields with Rabi frequencies $\varepsilon_{1,2}$ along the y direction. Two control fields $\Omega_{1,2}$ are applied to drive the atomic transitions $|1,2\rangle \leftrightarrow |3\rangle$ resonantly to form CPT. The atoms are in a superposition of ground states $|1,2\rangle$, i.e., the dark state. Two cavity fields $a_{1,2}$ and two external fields $\varepsilon_{1,2}$ are coupled to the atomic transitions $|1,2\rangle \leftrightarrow |4\rangle$ with the large detunings $\Delta_{1,2}$ and $\delta_{1,2}$, respectively.

$$H = H_{\rm CPT} + H_{\rm off}, \tag{2}$$

of which the first term

$$H_{\rm CPT} = \sum_{l=1,2} \hbar\Omega_l(\sigma_{3l} + \sigma_{l3}) \tag{3}$$

describes the resonant interactions of the atomic ensemble with the two control fields, and the second term,

$$H_{\rm off} = \sum_{l=1,2} \hbar(g_l a_l \sigma_{4l} e^{-i\Delta_l t} + g_l^* a_l^\dagger \sigma_{l4} e^{i\Delta_l t}) + \sum_{l=1,2} \hbar(\varepsilon_l \sigma_{4l} e^{-i\delta_l t} + \varepsilon_l^* \sigma_{l4} e^{i\delta_l t}), \tag{4}$$

represents the far off-resonant interactions of the atomic ensemble with the cavity fields and the external fields. Here g_l are the coupling strengths between the atomic ensemble and the cavity fields. $\Delta_l = \omega_{cl} - \omega_{4l}$ and $\delta_l = \nu_l - \omega_{4l}$ are the detunings of the cavity field frequencies ω_{cl} and the external field frequencies ν_l with respect to the corresponding atomic transition frequencies ω_{4l}, respectively.

III. CPT-BASED CAVITY-SPIN INTERACTION

Next we describe the far off-resonant interactions of the CPT atoms with the cavity fields and the external fields. It is convenient to merge the strong control fields into the atoms and to treat the atoms in terms of the dressed states. We assume that the Rabi frequencies of the control fields are much stronger than the atomic and cavity decay rates $\Omega_l \gg (\gamma_{3l}, \gamma_p, \kappa_l)(l = 1, 2)$. By diagonalizing $H_{\rm CPT}$, the dressed atomic states can be expressed in terms of the bare atomic states as

$$\begin{aligned} |D\rangle &= -\sin\theta|1\rangle + \cos\theta|2\rangle, \\ |+\rangle &= \frac{1}{\sqrt{2}}(\cos\theta|1\rangle + \sin\theta|2\rangle + |3\rangle), \\ |-\rangle &= \frac{1}{\sqrt{2}}(\cos\theta|1\rangle + \sin\theta|2\rangle - |3\rangle), \end{aligned} \tag{5}$$

where we have defined $\cos\theta = \frac{\Omega_1}{\Omega}$ and $\sin\theta = \frac{\Omega_2}{\Omega}$ with $\Omega = \sqrt{\Omega_1^2 + \Omega_2^2}$. In terms of the dressed atomic states, the Hamiltonian $H_{\rm CPT}$ can be rewritten as

$$H_{\rm CPT} = \hbar\Omega(\sigma_{++} - \sigma_{--}), \tag{6}$$

where $\sigma_{kl} = \sum_{\mu=1}^{N} |k^\mu\rangle\langle l^\mu|(k, l = D, +, -)$. The dressed states $|D\rangle$ and $|\pm\rangle$ are equally spaced and have their eigenvalues $\lambda_{D,\pm} = 0, \pm\hbar\Omega$.

Note that the state $|D\rangle$ consists of only the ground states but not the excited states. Spontaneous transitions happen only into $|D\rangle$ but not out of it. As a consequence, the atoms are trapped in it. Therefore, the state $|D\rangle$ is usually called the dark state. The steady-state populations are $\langle\sigma_{DD}\rangle = N$ and $\langle\sigma_{++}\rangle = \langle\sigma_{--}\rangle = 0$. In the CPT case, one has the maximal coherence $\langle\sigma_{12}\rangle = -\frac{N}{2}$. We also note that the other orthogonal superposition state $|B\rangle = \cos\theta|1\rangle + \sin\theta|2\rangle$, which acts as the component of the $|\pm\rangle$ states, is the bright state. In what follows, we will use both $|D\rangle$ and $|B\rangle$ as equivalent ones to the ground states $|1\rangle$ and $|2\rangle$.

Here the term $H_{\rm CPT}$ constitutes the free Hamiltonian for the dressed atom-field system. The dressed states are well separated from each other since $\Omega \gg (\gamma_{3l}, \gamma_{4l}, \gamma_p, \kappa_l)$. We can use the free Hamiltonian $H_{\rm CPT}$ to make a unitary transformation:

$$\tilde{H}_I(t) = e^{-\frac{i}{\hbar}H_{\rm CPT}t} H_{\rm off} e^{\frac{i}{\hbar}H_{\rm CPT}t}. \tag{7}$$

Since the atoms interact with the cavity fields and the external fields with the large detuning, the excited state $|4\rangle$ can be eliminated adiabatically. We follow the technique as in Ref. [90] and derive the effective interaction Hamiltonian:

$$H_{\rm eff} = -\frac{i}{\hbar}\tilde{H}_{\rm I}(t)\int_0^t dt'\tilde{H}_{\rm I}(t'). \tag{8}$$

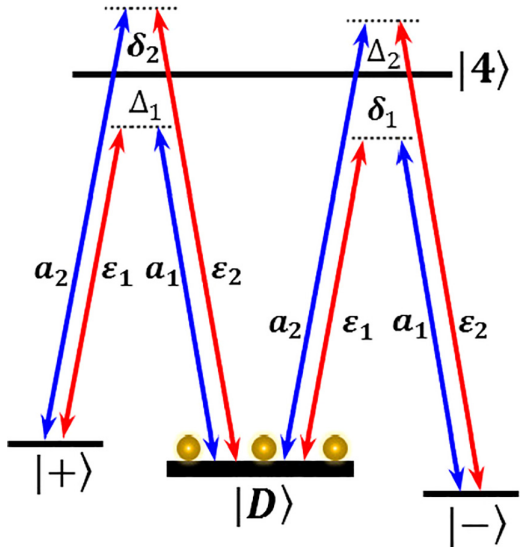

FIG. 2. Dressed atom-field interactions diagram. Two double off-resonance SRS interactions are induced between cavity fields $a_{1,2}$, external fields $\varepsilon_{1,2}$, and dressed atoms. The atoms are almost in a dark state $|D\rangle$.

Assuming $\Delta_1 = \delta_1 + \Omega$, $\Delta_2 = \delta_2 - \Omega$ and discarding the rapidly oscillating terms, we can obtain the effective interaction Hamiltonian,

$$\begin{aligned} H_{\rm eff} = \hbar[&G_1 a_1^\dagger(\sigma_{D+}\cosh r_1 + \sigma_{-D}\sinh r_1) - G_2 a_2^\dagger \\ &\times(\sigma_{D-}\cosh r_2 + \sigma_{+D}\sinh r_2)] + \text{H.c.}, \end{aligned} \tag{9}$$

where we have defined the effective coupling strengths $G_l = \frac{g|\varepsilon_l|\sin(2\theta)}{|\delta_l\Delta_l|}\sqrt{\frac{|\delta_l^2 - \Delta_l^2|}{8}}$ and the hyperbolic functions $\sinh r_l = \frac{|\Delta_l|}{\sqrt{|\delta_l^2 - \Delta_l^2|}}$, $\cosh r_l = \frac{|\delta_l|}{\sqrt{|\delta_l^2 - \Delta_l^2|}}$ $(l = 1, 2)$. Here $g_1^* = -g_2^* = g$ has been used. The interactions of the dressed spins with the cavity fields and the external fields are pictorially described in Fig. 2. The atoms are trapped in the dark state and two double off-resonance SRS interactions are induced between the dressed spins and the fields.

The dressed states $|\pm\rangle$ can be represented as a superposition of the bright state $|B\rangle$ and the excited state $|3\rangle$, i.e., $|\pm\rangle = \frac{1}{\sqrt{2}}(|B\rangle \pm |3\rangle)$. Then the effective interaction Hamiltonian can be rewritten as

$$\begin{aligned} H_{\rm eff} = \frac{\hbar}{\sqrt{2}}[&(G_1 a_1^\dagger\cosh r_1 - G_2 a_2^\dagger\cosh r_2 + G_1 a_1\sinh r_1 \\ &- G_2 a_2\sinh r_2)\sigma_{DB} + (G_1 a_1^\dagger\cosh r_1 + G_2 a_2^\dagger\cosh r_2 \\ &- G_1 a_1\sinh r_1 - G_2 a_2\sinh r_2)\sigma_{D3}] + \text{H.c.} \end{aligned} \tag{10}$$

The purpose of rewriting the Hamiltonian in this way is to make the physical mechanism of the spin squeezing clearer, as we will see later.

IV. SPIN SQUEEZING VIA DISSIPATION

Then we describe the characteristic effect of the cavity interaction on the ground state spin of the CPT atoms. Since we focus on the subspace of only the ground states $|1\rangle$ and $|2\rangle$, we define the Cartesian components $J = (J_x, J_y, J_z)$ of the

independent ground state spin as

$$J_x = J_{12} + J_{21}, \quad J_y = -i(J_{12} - J_{21}),$$
$$J_z = J_{11} - J_{22}. \tag{11}$$

The operators satisfy the SU(2) angular momentum commutation relations $[J_i, J_j] = 2i\varepsilon_{ijk}J_k$, where $\varepsilon_{ijk}(i, j, k = x, y, z)$ is the Levi-Civita symbol. Assuming the equal Rabi frequencies $\Omega_1 = \Omega_2$, i.e., $\sin\theta = \cos\theta = \frac{1}{\sqrt{2}}$, the spin components can be represented as

$$J_x = -(\sigma_{DD} - \sigma_{BB}), \quad J_y = i(\sigma_{DB} - \sigma_{DB}^\dagger),$$
$$J_z = -(\sigma_{DB} + \sigma_{DB}^\dagger). \tag{12}$$

For the dark resonance, we have their mean values $\langle J_x\rangle = -N$, $\langle J_y\rangle = \langle J_z\rangle = 0$. Therefore, the mean total spin is along the x direction.

The spin squeezing allows one to surpass SQL for phase estimation within Ramsey interferometry. To characterize the degree of spin squeezing, we introduce the spin-squeezing parameter [9,10]

$$\xi^2 = \frac{N(\delta J_\perp)^2_{\min}}{\langle J_x\rangle^2}, \tag{13}$$

where $(\delta J_\perp)^2_{\min} = (\langle J_\perp^2\rangle - \langle J_\perp\rangle^2)_{\min}$ is the minimum spin fluctuation in the direction perpendicular to the mean total spin J_x and $J_\perp = J_y\cos\phi + J_z\sin\phi(\phi \in [0, 2\pi])$. The optimal angle of squeezing can be derived as $\phi_m = \phi$ or $\phi_m = \frac{\pi}{2} - \phi$, where $\tan(2\phi) = \frac{\langle\delta J_x\delta J_z\rangle + \langle\delta J_z\delta J_y\rangle}{\langle(\delta J_y)^2\rangle - \langle(\delta J_z)^2\rangle}$. A state is a spin-squeezed state if $\xi^2 < 1$. The smaller ξ^2 indicates the stronger squeezing.

A. Numerical results

In numerical calculations, the atomic spontaneous emission rates are assumed to be the same, i.e., $\gamma_{31} = \gamma_{32} = \gamma$ and we use γ as the unit of the decay rates, the detunings, and the Rabi frequencies. The CPT atoms are constituted by the resonant interactions between the ground states $|1, 2\rangle$ and the excited state $|3\rangle$, and the large detuned interactions of the other fields with the CPT atoms have less effect on the CPT atoms. Therefore, the atoms are almost trapped in the dark state $|D\rangle$, and there is nearly no population on the bright state $|B\rangle$ and the excited state $|3\rangle$. In this case, the operators satisfy the commutation relations $[\sigma_{DB}, \sigma_{BD}] = [\sigma_{D3}, \sigma_{3D}] \approx N$ and $[\sigma_{3D}, \sigma_{DB}] = [\sigma_{BD}, \sigma_{D3}] \approx 0$. Following the standard technique [91–93], we derive the quantum Heisenberg-Langevin equations from Eq. (10) as

$$\dot\sigma_{DB} = -\left(\frac{\gamma}{2} + \frac{3}{8}\gamma_p\right)\sigma_{DB} + \frac{\gamma_p}{8}\sigma_{DB}^\dagger - \frac{iN}{\sqrt{2}}(G_1\cosh r_1 a_1 - G_2\cosh r_2 a_2 + G_1\sinh r_1 a_1^\dagger - G_2\sinh r_2 a_2^\dagger) + F_{\sigma_{DB}}(t), \tag{14}$$

$$\dot\sigma_{D3} = -\left(\frac{\gamma}{2} + \frac{3}{8}\gamma_p\right)\sigma_{D3} - \frac{\gamma_p}{8}\sigma_{D3}^\dagger - \frac{iN}{\sqrt{2}}(G_1\cosh r_1 a_1 + G_2\cosh r_2 a_2 - G_1\sinh r_1 a_1^\dagger - G_2\sinh r_2 a_2^\dagger) + F_{\sigma_{D3}}(t), \tag{15}$$

$$\dot a_1 = -\frac{\kappa_1}{2}a_1 - \frac{iG_1}{\sqrt{2}}[\cosh r_1(\sigma_{DB} + \sigma_{D3}) + \sinh r_1(\sigma_{DB}^\dagger - \sigma_{D3}^\dagger)] + F_{a_1}(t), \tag{16}$$

$$\dot a_2 = -\frac{\kappa_2}{2}a_2 - \frac{iG_2}{\sqrt{2}}[\cosh r_2(\sigma_{D3} - \sigma_{DB}) - \sinh r_2(\sigma_{D3}^\dagger + \sigma_{DB}^\dagger)] + F_{a_2}(t). \tag{17}$$

Here the noise terms F's satisfy correlations $\langle F_o(t)F_{o'}(t')\rangle = 2D_{oo'}\delta(t - t')$, where the nonzero diffusion coefficients are listed as $2D_{\sigma_{DB}\sigma_{DB}} = 2D_{\sigma_{DB}^\dagger\sigma_{DB}^\dagger} = -\frac{\gamma_p}{8}N$, $2D_{\sigma_{D3}\sigma_{D3}} = 2D_{\sigma_{D3}^\dagger\sigma_{D3}^\dagger} = \frac{\gamma_p}{8}N$, $2D_{\sigma_{DB}\sigma_{DB}^\dagger} = 2D_{\sigma_{D3}\sigma_{D3}^\dagger} = (\gamma + \frac{3}{4}\gamma_p)N$, $2D_{a_l a_l^\dagger} = \kappa_l(l = 1, 2)$. At steady state $\langle\sigma_{DB}\rangle = \langle\sigma_{D3}\rangle = \langle a_l\rangle = 0$, then $\delta\sigma_{DB} = \sigma_{DB}$, $\delta\sigma_{D3} = \sigma_{D3}$ and $\delta a_l = a_l$. To quantify the spin squeezing, we introduce the quadrature components as $\delta X_i = \frac{1}{\sqrt{2}}(\nu_i + \nu_i^\dagger)$, $\delta P_i = -\frac{i}{\sqrt{2}}(\nu_i - \nu_i^\dagger)$, $(\nu_1 = \sigma_{DB}, \nu_2 = \sigma_{D3}, \nu_3 = a_1, \nu_4 = a_2)$, and the noise quadratures F_{X_i} and F_{P_i} are defined in the same way. The quantum Heisenberg-Langevin equations of the quadrature fluctuations can be written as the matrix form

$$\dot u(t) = Au(t) + \zeta(t), \tag{18}$$

where the column vector for the fluctuation variables is arranged as $u(t) = (\delta X_1, \delta P_1, \delta X_2, \delta P_2, \delta X_3, \delta P_3, \delta X_4, \delta P_4)^T$, the corresponding noise terms are listed as $\zeta(t) = [F_{X_1}(t), F_{P_1}(t), F_{X_2}(t), F_{P_2}(t), F_{X_3}(t), F_{P_3}(t), F_{X_4}(t), \quad F_{P_4}(t)]^T$, and the drift matrix is given in Appendix B.

The system is stable only if all eigenvalues of the drift matrix A have negative real parts, which can be derived from the Routh-Hurwitz criterion [94]. In the following numerical calculations, the selected parameters satisfy the stability condition. Defining an 8×8 covariance matrix (CM) Q with components $Q_{ij}(t) = \frac{1}{2}\langle u_i(t)u_j(t) + u_j(t)u_i(t)\rangle$, $(i, j = 1, 2, \ldots, 8)$, we can derive a dynamical equation of the CM,

$$\dot Q(t) = AQ(t) + Q(t)A^T + D, \tag{19}$$

where the diffusion matrix is given by $D = \mathrm{diag}[N\Gamma_1, N\Gamma_2, N\Gamma_2, N\Gamma_1, \frac{\kappa_1}{2}, \frac{\kappa_1}{2}, \frac{\kappa_2}{2}, \frac{\kappa_2}{2}]$ and $\Gamma_{1,2}$ have been defined in Appendix B. The diffusion matrix D characterizing the noise correlations is defined through $D_{ij}\delta(t - t') = \frac{1}{2}\langle\zeta_i(t)\zeta_j(t') + \zeta_j(t')\zeta_i(t)\rangle$. The spin squeezing can be determined entirely by the elements of the CM.

The time evolutions of the spin-squeezing parameter ξ^2 are given in Fig. 3. To characterize the effect of system parameters on the spin squeezing, we define the two new parameters: the ratio of the effective coupling strength $s = \frac{G_1}{G_2}$ and the ratio of the squeezing parameter $q = \frac{r_1}{r_2}$. Figure 3(a) plots the time evolutions of ξ^2 for different s by taking parameters $\kappa_{1,2} = 10\gamma$, $\gamma_p = 0.01\gamma$, $\delta_1 = -\delta_2 = -10\gamma$, $\varepsilon_1 = 5\gamma$, $r_{1,2} = 1.5$, and $C_0 = 10^2$. Here $C_0 = \frac{g^2N}{\kappa\gamma}$ is defined as the cooperativity parameter. With the evolution of the time, the spin-squeezing parameter ξ^2 slows down and eventually tends to a stable value. For $s = 0.5$, the curve drops the fastest and the stable value is the smallest. When the cooperativity parameter is increased to $C_0 = 10^3$, as shown in Fig. 3(b), the spin-squeezing parameter ξ^2 becomes smaller and there is a weak oscillating behavior before reaching a stable value. It can be seen that the asymmetric effective coupling strength

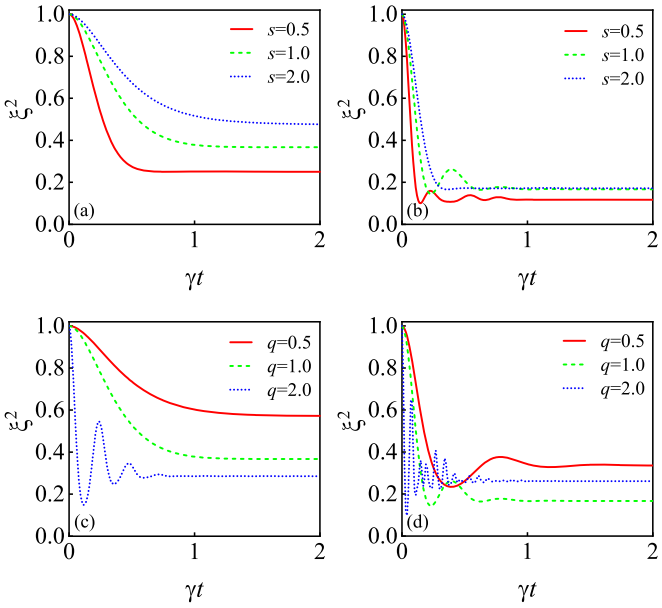

FIG. 3. Time evolution of the spin-squeezing parameter ξ^2. The parameter s is the ratio of the effective coupling strength, i.e., $s = \frac{G_1}{G_2}$. The parameter q is the ratio of the squeezing parameter, i.e., $q = \frac{r_1}{r_2}$. (a) $C_0 = 10^2$, $r_2 = 1.5$, $\delta_2 = 10\gamma$; (b) $C_0 = 10^3$, $r_2 = 1.5$, $\delta_2 = 10\gamma$; (c) $C_0 = 10^2$, $\varepsilon_2 = 5\gamma$; (d) $C_0 = 10^3$, $\varepsilon_2 = 5\gamma$. The other parameters are chosen as $\kappa_{1,2} = 10\gamma$, $\gamma_p = 0.01\gamma$, $\delta_1 = -10\gamma$, $\varepsilon_1 = 5\gamma$, $r_1 = 1.5$.

($s = 0.5$) can generate stronger steady spin squeezing than the symmetric effective coupling strength ($s = 1$). Figures 3(c) and 3(d) plot the time evolutions of ξ^2 for different q by setting parameters $\kappa_{1,2} = 10\gamma$, $\gamma_p = 0.01\gamma$, $\delta_1 = -10\gamma$, $\varepsilon_{1,2} = 5\gamma$, $r_1 = 1.5$, $C_0 = 10^2$, and $C_0 = 10^3$, respectively. When $C_0 = 10^2$, the parameter $q = 2$ corresponds to the best steady spin squeezing, but when C_0 is increased to 10^3, the parameter $q = 1$ corresponds to the best steady spin squeezing. Similar to Figs. 3(a) and 3(b), the large cooperativity parameter can lead to more pronounced oscillating behavior and the smaller stable spin-squeezing parameter.

Figure 4(a) gives the density plot of the stable spin-squeezing parameter ξ^2 versus the cooperativity parameter C_0 and the parameter s, and the corresponding 2D plot is shown in Fig. 4(b). As the cooperativity parameter C_0 increases, the spin-squeezing parameter ξ^2 decreases rapidly until it reaches a stable value. The constant value is the largest for $s = 1$, which means the spin squeezing is the weakest. This can also be seen from Fig. 4(a). Figure 4(b) shows that the best spin squeezing can reach 90%. Figure 4(c) is the density plot of the stable spin-squeezing parameter ξ^2 versus the squeezing parameter r_2 and the parameter q, and the corresponding 2D plot is given in Fig. 4(d). Figure 4(d) shows that with the increase of r_2, the spin-squeezing parameter ξ^2 first decreases to a minimum value and then gradually increases until the spin squeezing disappears. The best spin squeezing can be obtained at a certain value of r_2. When $q = 0.5$, the spin squeezing is the weakest and the squeezing range is the widest. In contrast, when $q = 2$, the spin squeezing is the strongest, about 90%. When $q = 1$, the squeezing range is the narrowest, which can also be seen intuitively in Fig. 4(c).

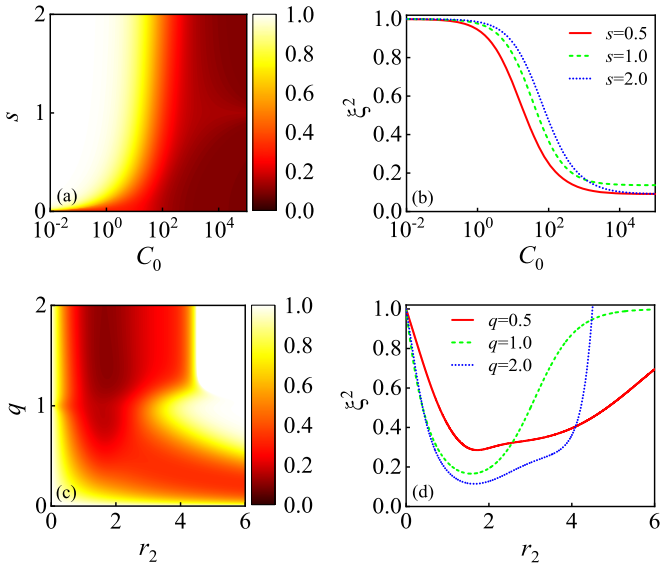

FIG. 4. Density plot (a) and 2D plot (b) of the spin-squeezing parameter ξ^2 versus the cooperativity parameter C_0 and the parameter s. Taking parameters $\varepsilon_1 = 5\gamma$, $r_{1,2} = 1.5$. Density plot (c) and 2D plot (d) of the spin-squeezing parameter ξ^2 versus the squeezing parameter r_2 and the parameter q. Taking parameters $\varepsilon_{1,2} = 5\gamma$, $C_0 = 10^3$. The other parameters are the same as in Fig. 3.

Figure 5(a) shows the density plot of the stable spin-squeezing parameter ξ^2 versus the squeezing parameter r and the cooperativity parameter C_0. The spin-squeezing parameter ξ^2 versus C_0 for different r is plotted in Fig. 5(b). Here we consider the symmetric parameters and take $\kappa_{1,2} = 10\gamma$, $\gamma_p = 0.01\gamma$, $\delta_1 = -\delta_2 = -10\gamma$, $\varepsilon_{1,2} = 5\gamma$, $r_{1,2} = r$,

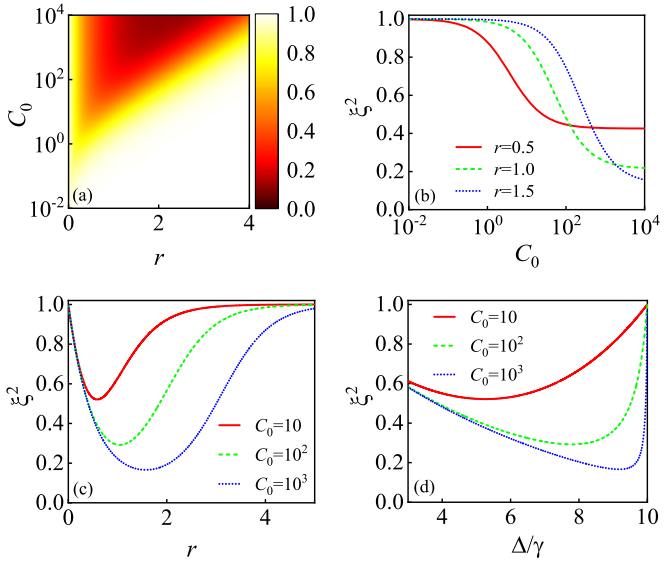

FIG. 5. (a) Density plot of the spin-squeezing parameter ξ^2 versus the squeezing parameter r and the cooperativity parameter C_0. (b) The spin-squeezing parameter ξ^2 versus C_0 for different r. (c) The spin-squeezing parameter ξ^2 versus r for different C_0. (d) The spin-squeezing parameter ξ^2 versus Δ/γ for different C_0. The parameters are chosen as $\kappa_{1,2} = 10\gamma$, $\gamma_p = 0.01\gamma$, $\delta_1 = -\delta_2 = -10\gamma$, $\varepsilon_{1,2} = 5\gamma$, $r_{1,2} = r$, $\Delta_1 = -\Delta_2 = -\Delta$.

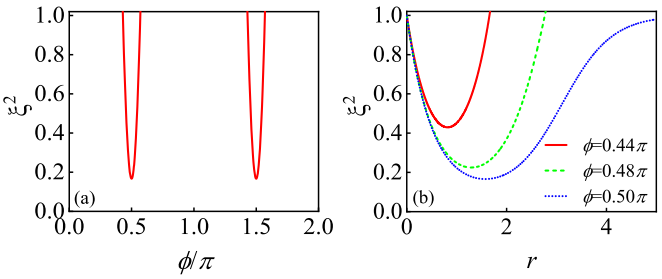

FIG. 6. (a) The spin-squeezing parameter ξ^2 versus the angle ϕ/π. Setting the parameter $r = 1.5$. (b) The spin-squeezing parameter ξ^2 versus the squeezing parameter r for different ϕ. The parameters are taken as $C_0 = 10^3$, $r_{1,2} = r$. The other parameters are the same as in Fig. 5.

$\Delta_1 = -\Delta_2 = -\Delta$. As the cooperativity parameter C_0 increases, the spin-squeezing parameter ξ^2 decreases slowly and tends to a stable value. The magnitude of this stable value is related to r. Figure 5(c) gives the spin-squeezing parameter ξ^2 versus r for different C_0. When increasing r, the spin-squeezing parameter ξ^2 first decreases to a minimum value, then increases, and finally the spin squeezing disappears. The best spin squeezing can be obtained for a moderate value of r. Fig. 5(d) plots the spin-squeezing parameter ξ^2 versus Δ/γ for different C_0. When Δ increases, the spin-squeezing parameter slowly decreases to a minimum value and then increases rapidly. Note that if Δ is too small, the cavity field is in near resonance with the excited state $|4\rangle$ and more atoms get excited. In this case, the spontaneous emission from the excited state may destroy the spin squeezing. Therefore, to avoid the atomic excitation, Δ is taken to be at least larger than 3γ, as shown in Fig. 5(d). The best spin squeezing in Fig. 5 is about 85%.

Figure 6(a) gives the spin-squeezing parameter ξ^2 versus the angle ϕ/π. It is clear that the spin squeezing varies periodically with ϕ/π, and the degree of spin squeezing is the best at $\phi = 0.5\pi$ and $\phi = 1.5\pi$. Figure 6(b) plots the spin-squeezing parameter ξ^2 versus the squeezing parameter r for different ϕ. For the case of $\phi = 0.5\pi$, we achieve the strongest spin squeezing, about 85%. As r increases, the spin squeezing first increases, then decreases, and eventually disappears. The best spin squeezing can be obtained when r takes a moderate value.

B. Approximate analytic solutions

To measure the degree of squeezing, it is better to find the expression for the spin-squeezing parameter under appropriate approximations. Assuming that the system parameters are symmetric, i.e., $\kappa_{1,2} = \kappa$, $r_{1,2} = r$, $G_{1,2} = G$, the Heisenberg-Langevin equations for the spin operators σ_{DB} and σ_{D3} can be simplified from Eqs. (14) and (15) to

$$\dot{\sigma}_{DB} = -\frac{\gamma}{2}\sigma_{DB} - iGN(d\cosh r + d^\dagger \sinh r) + F_{\sigma_{DB}}(t), \tag{20}$$

$$\dot{\sigma}_{D3} = -\frac{\gamma}{2}\sigma_{D3} - iGN(c\cosh r - c^\dagger \sinh r) + F_{\sigma_{D3}}(t), \tag{21}$$

where we have defined the collection cavity sum mode $c = \frac{1}{\sqrt{2}}(a_1 + a_2)$ and the difference mode $d = \frac{1}{\sqrt{2}}(a_1 - a_2)$. Here the effect of γ_p has been ignored because $\gamma \gg \gamma_p$. It can be seen that σ_{DB} is coupled only to the collection difference mode d and the decoupling between σ_{DB} and σ_{D3} occurs.

An effective Hamiltonian for the spin interaction is obtained from the coherent terms in Eq. (20) when the incoherent terms are temporarily dropped, as

$$H_{\text{eff}} = \hbar G d^\dagger(\sigma_{DB}\cosh r + \sigma_{DB}^\dagger \sinh r) + \text{H.c.} \tag{22}$$

The effective Hamiltonian describes the transition between the dark state $|D\rangle$ and the bright state $|B\rangle$, creating or annihilating a collective cavity mode d.

We now consider the case of $N \to \infty$, so the dynamics of the collective spin can be mapped to a bosonic mode $\sigma_{DB}/\sqrt{N}$. Here, we have assumed that the atoms are almost in the dark state $|D\rangle$ and the atomic number of the bright state $|B\rangle$ is much smaller than the total number N, i.e., $\langle\sigma_{DB}^\dagger\sigma_{DB}\rangle \ll N$, and have made the spin-wave approximation. The effective Hamiltonian is correspondingly transformed to

$$H_{\text{eff}} = \hbar G(d^\dagger\beta + \beta^\dagger d), \tag{23}$$

where β is the collective Bogoliubov mode, which is defined as

$$\beta = \sigma_{DB}\cosh r + \sigma_{DB}^\dagger \sinh r. \tag{24}$$

The dissipation of the collective cavity mode d can drive the mode β to its vacuum state, which corresponds to the squeezing vacuum state of the mode σ_{DB}.

Following the standard technique [91–93], we derive the quantum Heisenberg-Langevin equations from Eq. (23) as

$$\begin{aligned}\dot{\beta} &= -\frac{\gamma}{2}\beta - iGNd + \cosh r F_{\sigma_{DB}}(t) + \sinh r F_{\sigma_{DB}^\dagger}(t),\\ \dot{d} &= -\frac{\kappa}{2}d - iG\beta + \frac{1}{\sqrt{2}}[F_{a_1}(t) - F_{a_2}(t)].\end{aligned} \tag{25}$$

If the cavity dissipation is sufficiently large, the collective cavity mode can be eliminated adiabatically. Then the Heisenberg-Langevin equation for the mode β can be derived as

$$\dot{\beta} = -\frac{\gamma}{2}(1 + C)\beta + F(t), \tag{26}$$

where $C = \frac{4G^2N}{\kappa\gamma}$ is the effective cooperativity parameter, and the noise term is represented as

$$\begin{aligned}F(t) = &\cosh r F_{\sigma_{DB}}(t) + \sinh r F_{\sigma_{DB}^\dagger}(t)\\ &- \frac{i\sqrt{2}GN}{\kappa}[F_{a_1}(t) - F_{a_2}(t)].\end{aligned} \tag{27}$$

In Eq. (26), $\frac{\gamma}{2}$ is the atomic decay rate by the vacuum reservoir, $\frac{\gamma C}{2}$ is the cavity-induced damping rate, and $F(t)$ includes the atomic and cavity noise fluctuations.

The spin components J_y and J_z are expressed in terms of the β mode as $J_y = ie^r(\beta - \beta^\dagger)$, $J_z = -e^{-r}(\beta + \beta^\dagger)$, then the dynamical equations of the spin variances are derived as

$$\begin{aligned}\frac{d}{dt}\langle J_y^2\rangle &= -\gamma(1 + C)\langle J_y^2\rangle + N\gamma(1 + Ce^{2r}),\\ \frac{d}{dt}\langle J_z^2\rangle &= -\gamma(1 + C)\langle J_z^2\rangle + N\gamma(1 + Ce^{-2r}),\\ \frac{d}{dt}\langle J_zJ_y + J_yJ_z\rangle &= -\gamma(1 + C)\langle J_zJ_y + J_yJ_z\rangle.\end{aligned} \tag{28}$$

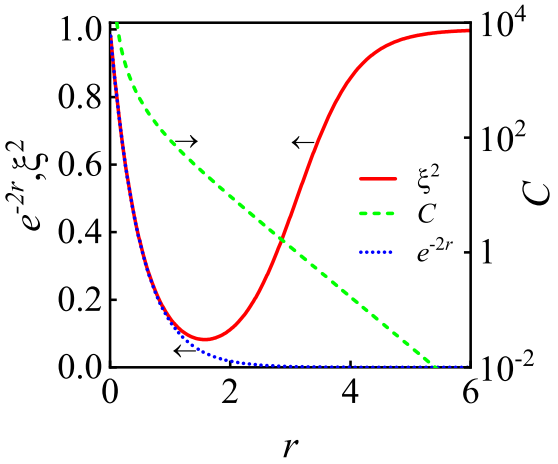

FIG. 7. The spin-squeezing parameter ξ^2 (solid line), the effective cooperativity parameter C (dashed line), and the squeezed factor e^{-2r} (dotted line) versus the squeezing parameter r. The parameters are chosen as $\gamma_p = 0$, $\delta_1 = -\delta_2 = -10\gamma$, $\varepsilon_{1,2} = 5\gamma$, $r_{1,2} = r$, $C_0 = 10^3$.

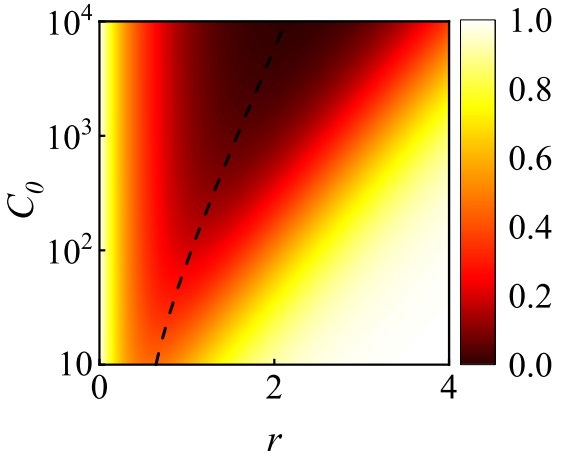

FIG. 8. Density plot of the spin-squeezing parameter ξ^2 versus the squeezing parameter r and the cooperativity parameter C_0. The black dashed line corresponds to Eq. (33). The other parameters are the same as in Fig. 7.

The solutions to these differential equations are

$$\langle J_y^2 \rangle = \frac{e^{-\gamma(1+C)t} + N\gamma(1+Ce^{2r})}{\gamma(1+C)},$$
$$\langle J_z^2 \rangle = \frac{e^{-\gamma(1+C)t} + N\gamma(1+Ce^{-2r})}{\gamma(1+C)},$$
$$\langle J_z J_y + J_y J_z \rangle = e^{-\gamma(1+C)t}. \tag{29}$$

It can be seen from the above expressions that the direction of the optimal squeezing (minimal variance) varies with time t and the minimal variance in the yz plane can be directly calculated via $(\delta J_\perp)^2_{\min} = \frac{1}{2}[\langle J_y^2 \rangle + \langle J_z^2 \rangle - \sqrt{(\langle J_y^2 \rangle - \langle J_z^2 \rangle)^2 + \langle J_z J_y + J_y J_z \rangle^2}]$ [8]. Finally, using the results of Eqs. (29), the spin-squeezing parameter is obtained from Eq. (13) as

$$\xi^2 = \frac{e^{-\gamma(1+C)t} + N\gamma(1+Ce^{-2r})}{N\gamma(1+C)}. \tag{30}$$

When $t \to \infty$, the spin-squeezing parameter of Eq. (30) can be expressed as

$$\xi^2 = \frac{1+Ce^{-2r}}{1+C}. \tag{31}$$

Obviously, the spin-squeezing parameter ξ^2 is determined by the ideal squeezed factor e^{-2r} and the effective cooperativity parameter C. Figure 7 plots the spin-squeezing parameter ξ^2, the effective cooperativity parameter C, and the squeezed factor e^{-2r} versus the squeezing parameter r. In general, the larger the squeezing parameter r, the greater the spin squeezing will be. However, the effective cooperativity parameter C is associated with the effective coupling strength G. With the increase of the squeezing parameter r, the effective coupling strength G decreases, resulting in the decrease of the effective cooperativity parameter C. This effectively inhibits the atomic reservoir effect and reduces the spin squeezing. Therefore, with the increase of r, the spin squeezing first increases to the maximum and then gradually decreases. The best spin squeezing occurs at a moderate value of r. Finally, optimizing ξ^2 with respect to r, we can obtain the optimal spin-squeezing parameter

$$\xi^2_{\text{opt}} = \frac{2Y+2}{Y(2+\sqrt{Y+2})+2} \tag{32}$$

at

$$r_{\text{opt}} = \tfrac{1}{2}\ln(1+\sqrt{Y+2}), \tag{33}$$

where $Y = \frac{2C_0\varepsilon_L^2}{|\delta_l|^2}$. Figure 8 shows the density plot of the spin-squeezing parameter ξ^2 versus the squeezing parameter r and the cooperativity parameter C_0. The black dashed line corresponds to Eq. (33). As C_0 increases, r_{opt} increases and the degree of the spin squeezing also increases significantly.

Figure 9 shows the analytical and numerical results of the spin-squeezing parameter ξ^2 versus the squeezing parameter r. The analytical and numerical results are according to Eqs. (19) and (31), respectively. We choose different cavity

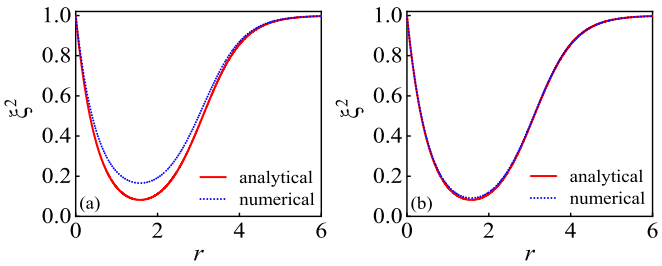

FIG. 9. Analytical (solid line) and numerical (dotted line) results of the spin-squeezing parameter ξ^2 versus the squeezing parameter r. The analytical and numerical results are according to Eqs. (19) and (31), respectively. Taking the parameters (a) $\kappa_{1,2} = 10\gamma$ and (b) $\kappa_{1,2} = 100\gamma$. The other parameters are the same as in Fig. 7.

decay rates: (a) $\kappa_{1,2} = 10\gamma$ and (b) $\kappa_{1,2} = 100\gamma$. The other parameters are taken as $\gamma_p = 0$, $\delta_1 = -\delta_2 = -10\gamma$, $\varepsilon_{1,2} = 5\gamma$, $r_{1,2} = r$, $C_0 = 10^3$. It can be seen from Fig. 9 that the analytical results are valid under the adiabatic condition $\kappa_{1,2} \gg \gamma$ and independent of $\kappa_{1,2}$. However, the numerical results are dependent on $\kappa_{1,2}$. When $\kappa_{1,2} = 10\gamma$, there is a deviation between the analytical and numerical results, which is less than 10%, as shown in Fig. 9(a). If $\kappa_{1,2}$ are increased to 100γ, the analytical results are very in agreement with the numerical results, as shown in Fig. 9(b). In this case, the best spin squeezing is about 90%.

In comparison with previous studies on the spin squeezing [69–84], our scheme exhibits the following significant characteristics: (i) Previous proposals mostly relied on the far-off-resonant interactions, where the atoms are hardly excited and the spontaneous emission is immune. In contrast, our approach exploits a resonantly interacting system to generate the spin squeezing, in which the atoms are trapped in the dark state and the spontaneous emission is eliminated in destructive interference. (ii) Different from the previous experimental schemes which apply a $\frac{\pi}{2}$ microwave pulse to prepare an equal superposition of two ground states, our scheme directly uses quantum interference effects to produce a maximum coherent state of the two ground states with no need of the preparation of the initial spin state. (iii) Our scheme exploits the dissipation mechanism of cavity reservoir to generate the atomic spin squeezed state. Therefore, the resulting spin squeezing is stable and deterministic, does not require the initial preparation of the nonclassical states, and is robust against the environmental noise.

C. Experimental implementations

Finally, we give a discussion on the experimental feasibility. In recent years, a large number of experimental investigations on the spin squeezing via the atom-field interactions have been performed in different quantum optics systems [4–6,25,57–60]. For example, Schleier-Smith *et al.* obtained the initial spin state by optical pumping the ensemble into the ground state followed by applying a $\frac{\pi}{2}$ microwave pulse, and then induced conditional spin squeezing by employing two probe light pulses and a π microwave pulse to the initial spin state [5]. Leroux *et al.* demonstrated a method for deterministically generating squeezed states using switchable light-mediated interactions in a dilute ensemble of otherwise noninteracting atoms [6]. On the other hand, Krauter *et al.* reported on an experiment where dissipation continuously generates entanglement between two macroscopic objects by using atomic tomography via quantum polarization spectroscopy [95].

The present scheme contains an atomic ensemble, a two-mode optical cavity, and four classical laser beams. It is well-known that rubidium is an alkali metal element with univalent positron and relatively simple electronic structure for experimental control. The preparation of cold Rb atoms has been well demonstrated experimentally. In our scheme, to access the spin squeezed state in experiments, the CPT atoms need to be prepared first. The two strong control fields with linearly polarized light couple resonant pairs of hyperfine sublevels of electronic ground-state Rb atoms via the excited state [96]. In this case, one has a maximum coherent state of the two ground states. Second, switching on a two-mode optical cavity and the other two classical laser beams to induce the spin squeezing by large detuned interactions with the CPT atoms. Finally, a weak probe field is used to verify the atomic spin squeezed state by detecting the photon numbers of the transmitted probe field. An ensemble of ^{87}Rb atoms can be used effectively in our scheme, in which the D_1 line serves for the double Λ configuration with $|1\rangle = |5^2S_{1/2}, F = 1\rangle$, $|2\rangle = |5^2S_{1/2}, F = 2\rangle$, $|3\rangle = |5^2P_{1/2}, F = 1\rangle$, and $|4\rangle = |5^2P_{1/2}, F = 2\rangle$. As shown in Fig. 1, an ensemble of $N \sim 10^6$ cold ^{87}Rb atoms is placed inside the two-mode optical cavity along the x direction, and the four classical laser beams are, respectively, along the y and z directions. The frequencies of the cavity fields can be adjusted flexibly to ensure the far-detuned interactions with the atomic ensemble, and their decay rates should be large enough to validate the adiabatic elimination of the cavity fields. We can take the cavity loss $\kappa_{1,2} = 10\gamma$, the atom-cavity coupling coefficient $g_{1,2} = 0.1\gamma$, and then the cooperativity parameter is $C_0 = 10^3$. When the two cavity fields and the two external fields have antisymmetric detunings with the atomic transitions, i.e., $\delta_1 = -\delta_2$, $\Delta_1 = -\Delta_2$, the condition $\Delta_1 = \delta_1 + \Omega$, $\Delta_2 = \delta_2 - \Omega$ can be satisfied. In this case, there are the two same squeezing parameters $r_1 = r_2$. In addition, the squeezing parameters can be changed by adjusting the detunings and the Rabi frequencies of the control fields. In general, this scheme is feasible and very convenient to control in experiments.

V. CONCLUSION

In conclusion, we have shown that the cavity dissipation-induced spin squeezing in CPT can almost approach 85%-90%. When two control fields are tuned to resonantly drive the atomic transitions between the two ground states and one excited state, the atoms are trapped in the dark state and one has the maximal coherence. The dispersion interactions between the two cavity fields, the two external fields, and the dressed atoms induce two double off-resonance SRS interactions between the atomic dressed states. The cavity dissipative quantum dynamical process can be established after the excited state is adiabatically eliminated. The cavity dissipation plays an active role for generating the steady spin squeezed state. Furthermore, the parameter regimes are given by numerical calculation and the physical mechanism is analyzed under reasonable approximation. Our paper provides an option for preparing the spin squeezed state, which has potential applications in high-precision measurements, quantum information processing, and quantum computing.

ACKNOWLEDGMENT

This work is supported by the National Natural Science Foundation of China (Grants No. 12274164 and No. 61875067) and the Fundamental Research Funds for the Central Universities (Grant No. CCNU24JC017).

APPENDIX A: THE DAMPING RATES IN TERMS OF THE ATOM-FIELD SYSTEM

The dissipation term Γ_o of the atom-field system can be written as

$$\begin{aligned}
\Gamma_{\sigma_{12}} &= \gamma_p, \\
\Gamma_{\sigma_{13}} &= \Gamma_{\sigma_{23}} = \frac{\gamma_{31}}{2} + \frac{\gamma_{32}}{2} + \frac{\gamma_p}{4}, \\
\Gamma_{\sigma_{14}} &= \Gamma_{\sigma_{24}} = \frac{\gamma_{41}}{2} + \frac{\gamma_{42}}{2} + \frac{\gamma_p}{4}, \\
\Gamma_{\sigma_{33}} &= \gamma_{31} + \gamma_{32}, \\
\Gamma_{\sigma_{34}} &= \frac{\gamma_{31}}{2} + \frac{\gamma_{32}}{2} + \frac{\gamma_{41}}{2} + \frac{\gamma_{42}}{2}, \\
\Gamma_{\sigma_{44}} &= \gamma_{41} + \gamma_{42}, \\
\Gamma_{a_1} &= \frac{\kappa_1}{2}, \Gamma_{a_2} = \frac{\kappa_2}{2}.
\end{aligned} \tag{A1}$$

APPENDIX B: THE DRIFT MATRIX

The drift matrix in the quantum Heisenberg-Langevin equations of the quadrature fluctuations reads

$$A = \begin{pmatrix}
-\Gamma_1 & 0 & 0 & 0 & 0 & \frac{G_1 N}{\sqrt{2}} e^{-r_1} & 0 & -\frac{G_2 N}{\sqrt{2}} e^{-r_2} \\
0 & -\Gamma_2 & 0 & 0 & -\frac{G_1 N}{\sqrt{2}} e^{r_1} & 0 & \frac{G_2 N}{\sqrt{2}} e^{r_2} & 0 \\
0 & 0 & -\Gamma_2 & 0 & 0 & \frac{G_1 N}{\sqrt{2}} e^{r_1} & 0 & \frac{G_2 N}{\sqrt{2}} e^{r_2} \\
0 & 0 & 0 & -\Gamma_1 & -\frac{G_1 N}{\sqrt{2}} e^{-r_1} & 0 & -\frac{G_2 N}{\sqrt{2}} e^{-r_2} & 0 \\
0 & \frac{G_1}{\sqrt{2}} e^{-r_1} & 0 & \frac{G_1}{\sqrt{2}} e^{r_1} & -\frac{\kappa_1}{2} & 0 & 0 & 0 \\
-\frac{G_1}{\sqrt{2}} e^{r_1} & 0 & -\frac{G_1}{\sqrt{2}} e^{-r_1} & 0 & 0 & -\frac{\kappa_1}{2} & 0 & 0 \\
0 & -\frac{G_2}{\sqrt{2}} e^{-r_2} & 0 & \frac{G_2}{\sqrt{2}} e^{r_2} & 0 & 0 & -\frac{\kappa_2}{2} & 0 \\
\frac{G_2}{\sqrt{2}} e^{r_2} & 0 & -\frac{G_2}{\sqrt{2}} e^{-r_2} & 0 & 0 & 0 & 0 & -\frac{\kappa_2}{2}
\end{pmatrix}, \tag{B1}$$

where $\Gamma_1 = \frac{\gamma}{2} + \frac{\gamma_p}{4}$, $\Gamma_2 = \frac{\gamma}{2} + \frac{\gamma_p}{2}$.

[1] V. Giovannetti, S. Lloyd, and L. Maccone, Quantum-enhanced measurements: Beating the standard quantum limit, Science **306**, 1330 (2004).

[2] L. Pezzè, A. Smerzi, M. K. Oberthaler, R. Schmied, and P. Treutlein, Quantum metrology with nonclassical states of atomic ensembles, Rev. Mod. Phys. **90**, 035005 (2018).

[3] J. Estève, C. Gross, A. Weller, S. Giovanazzi, and M. K. Oberthaler, Squeezing and entanglement in a Bose-Einstein condensate, Nature (London) **455**, 1216 (2008).

[4] J. Appel, P. J. Windpassinger, D. Oblak, U. B. Hoff, N. Kjærgaard, and E. S. Polzik, Mesoscopic atomic entanglement for precision measurements beyond the standard quantum limit, Proc. Natl. Acad. Sci. USA **106**, 10960 (2009).

[5] M. H. Schleier-Smith, I. D. Leroux, and V. Vuletić, States of an ensemble of two-level atoms with reduced quantum uncertainty, Phys. Rev. Lett. **104**, 073604 (2010).

[6] I. D. Leroux, M. H. Schleier-Smith, and V. Vuletić, Implementation of cavity squeezing of a collective atomic spin, Phys. Rev. Lett. **104**, 073602 (2010).

[7] M. Kitagawa and M. Ueda, Squeezed spin states, Phys. Rev. A **47**, 5138 (1993).

[8] J. Ma, X. Wang, C. P. Sun, and F. Nori, Quantum spin squeezing, Phys. Rep. **509**, 89 (2011).

[9] D. J. Wineland, J. J. Bollinger, W. M. Itano, F. L. Moore, and D. J. Heinzen, Spin squeezing and reduced quantum noise in spectroscopy, Phys. Rev. A **46**, R6797(R) (1992).

[10] D. J. Wineland, J. J. Bollinger, W. M. Itano, and D. J. Heinzen, Squeezed atomic states and projection noise in spectroscopy, Phys. Rev. A **50**, 67 (1994).

[11] J. J. Bollinger, W. M. Itano, D. J. Wineland, and D. J. Heinzen, Optimal frequency measurements with maximally correlated states, Phys. Rev. A **54**, R4649(R) (1996).

[12] G. S. Agarwal and M. O. Scully, Ramsey spectroscopy with nonclassical light sources, Phys. Rev. A **53**, 467 (1996).

[13] P. R. Berman, *Atom Interferometry* (Academic, New York, 1997).

[14] G. Xu and D. J. Heinzen, State-selective Rabi and Ramsey magnetic resonance line shapes, Phys. Rev. A **59**, R922(R) (1999).

[15] D. Döring, G. McDonald, J. E. Debs, C. Figl, P. A. Altin, H. A. Bachor, N. P. Robins, and J. D. Close, Quantum-projection-noise-limited interferometry with coherent atoms in a Ramsey-type setup, Phys. Rev. A **81**, 043633 (2010).

[16] M. Xu and M. J. Holland, Conditional Ramsey spectroscopy with synchronized atoms, Phys. Rev. Lett. **114**, 103601 (2015).

[17] R. K. Altmann, S. Galtier, L. S. Dreissen, and K. S. E. Eikema, High-precision Ramsey-comb spectroscopy at deep ultraviolet wavelengths, Phys. Rev. Lett. **117**, 173201 (2016).

[18] C. Sanner, N. Huntemann, R. Lange, C. Tamm, and E. Peik, Autobalanced Ramsey spectroscopy, Phys. Rev. Lett. **120**, 053602 (2018).

[19] B. K. Malia, J. Martínez-Rincón, Y. Wu, O. Hosten, and M. A. Kasevich, Free space Ramsey spectroscopy in rubidium with noise below the quantum projection limit, Phys. Rev. Lett. **125**, 043202 (2020).

[20] R. G. Bullis, C. Rasor, W. L. Tavis, S. A. Johnson, M. R. Weiss, and D. C. Yost, Ramsey spectroscopy of the $2S_{1/2}$ hyperfine interval in atomic hydrogen, Phys. Rev. Lett. **130**, 203001 (2023).

[21] D. Oblak, P. G. Petrov, C. L. Garrido Alzar, W. Tittel, A. K. Vershovski, J. K. Mikkelsen, J. L. Sørensen, and E. S. Polzik, Quantum-noise-limited interferometric measurement of atomic noise: Towards spin squeezing on the Cs clock transition, Phys. Rev. A **71**, 043807 (2005).

[22] A. Sørensen and K. Mølmer, Spin-spin interaction and spin squeezing in an optical lattice, Phys. Rev. Lett. **83**, 2274 (1999).

[23] D. Meiser, J. Ye, and M. J. Holland, Spin squeezing in optical lattice clocks via lattice-based QND measurements, New J. Phys. **10**, 073014 (2008).

[24] A. Andre, A. S. Sørensen, and M. D. Lukin, Stability of atomic clocks based on entangled atoms, Phys. Rev. Lett. **92**, 230801 (2004).

[25] I. D. Leroux, M. H. Schleier-Smith, and V. Vuletic, Orientation-dependent entanglement lifetime in a squeezed atomic clock, Phys. Rev. Lett. **104**, 250801 (2010).

[26] J. Borregaard and A. S. Sørensen, Near-Heisenberg-limited atomic clocks in the presence of decoherence, Phys. Rev. Lett. **111**, 090801 (2013).

[27] J. Borregaard and A. S. Sørensen, Efficient atomic clocks operated with several atomic ensembles, Phys. Rev. Lett. **111**, 090802 (2013).

[28] I. Kruse, K. Lange, J. Peise, B. Lücke, L. Pezzè, J. Arlt, W. Ertmer, C. Lisdat, L. Santos, A. Smerzi, and C. Klempt, Improvement of an atomic clock using squeezed vacuum, Phys. Rev. Lett. **117**, 143004 (2016).

[29] E. Pedrozo-Peñafiel, S. Colombo, C. Shu, A. F. Adiyatullin, Z. Li, E. Mendez, B. Braverman, A. Kawasaki, D. Akamatsu, Y. Xiao, and V. Vuletiá, Entanglement on an optical atomic-clock transition, Nature (London) **588**, 414 (2020).

[30] B. C. Nichol, R. Srinivas, D. P. Nadlinger, P. Drmota, D. Main, G. Araneda, C. J. Ballance, and D. M. Lucas, An elementary quantum network of entangled optical atomic clocks, Nature (London) **609**, 689 (2022).

[31] G. D. Martinez, C. Li, A. Staron, J. Kitching, C. Raman, and W. R. McGehee, A chip-scale atomic beam clock, Nat. Commun. **14**, 3501 (2023).

[32] J. Geremia, J. K. Stockton, A. C. Doherty, and H. Mabuchi, Quantum Kalman filtering and the Heisenberg limit in atomic magnetometry, Phys. Rev. Lett. **91**, 250801 (2003).

[33] M. Vengalattore, J. M. Higbie, S. R. Leslie, J. Guzman, L. E. Sadler, and D. M. Stamper-Kurn, High-resolution magnetometry with a spinor Bose-Einstein condensate, Phys. Rev. Lett. **98**, 200801 (2007).

[34] P. Cappellaro and M. D. Lukin, Quantum correlation in disordered spin systems: Applications to magnetic sensing, Phys. Rev. A **80**, 032311 (2009).

[35] W. Wasilewski, K. Jensen, H. Krauter, J. J. Renema, M. V. Balabas, and E. S. Polzik, Quantum noise limited and entanglement-assisted magnetometry, Phys. Rev. Lett. **104**, 133601 (2010).

[36] M. Koschorreck, M. Napolitano, B. Dubost, and M. W. Mitchell, Sub-projection-noise sensitivity in broadband atomic magnetometry, Phys. Rev. Lett. **104**, 093602 (2010).

[37] G. de Lange, D. Ristè, V. V. Dobrovitski, and R. Hanson, Single-spin magnetometry with multipulse sensing sequences, Phys. Rev. Lett. **106**, 080802 (2011).

[38] K. Fang, V. M. Acosta, C. Santori, Z. Huang, K. M. Itoh, H. Watanabe, S. Shikata, and R. G. Beausoleil, High-sensitivity magnetometry based on quantum beats in diamond nitrogen-vacancy centers, Phys. Rev. Lett. **110**, 130802 (2013).

[39] D. Sheng, S. Li, N. Dural, and M. V. Romalis, Subfemtotesla scalar atomic magnetometry using multipass cells, Phys. Rev. Lett. **110**, 160802 (2013).

[40] K. Jensen, N. Leefer, A. Jarmola, Y. Dumeige, V. M. Acosta, P. Kehayias, B. Patton, and D. Budker, Cavity-enhanced room-temperature magnetometry using absorption by nitrogen-vacancy centers in diamond, Phys. Rev. Lett. **112**, 160802 (2014).

[41] W. Muessel, H. Strobel, D. Linnemann, D. B. Hume, and M. K. Oberthaler, Scalable spin squeezing for quantum-enhanced magnetometry with Bose-Einstein condensates, Phys. Rev. Lett. **113**, 103004 (2014).

[42] K. Arai, J. Lee, C. Belthangady, D. R. Glenn, H. Zhang, and R. L. Walsworth, Geometric phase magnetometry using a solid-state spin, Nat. Commun. **9**, 4996 (2018).

[43] X. Meng, Y. Zhang, X. Zhang, S. Jin, T. Wang, L. Jiang, L. Xiao, S. Jia, and Y. Xiao, Machine learning assisted vector atomic magnetometry, Nat. Commun. **14**, 6105 (2023).

[44] D. F. Walls and P. Zoller, Enhanced sensitivity of a gravitational-wave detector, Phys. Lett. A **85**, 118 (1981).

[45] K. Goda, O. Miyakawa, E. E. Mikhailov, S. Saraf, R. Adhikari, K. McKenzie, R. Ward, S. Vass, A. J. Weinstein, and N. Mavalvala, A quantum-enhanced prototype gravitational-wave detector, Nat. Phys. **4**, 472 (2008).

[46] J. Aasi, J. Abadie, B. P. Abbott, R. Abbott, T. D. Abbott, M. R. Abernathy, C. Adams, T. Adams, P. Addesso, R. X. Adhikari *et al.*, Enhanced sensitivity of the LIGO gravitational wave detector by using squeezed states of light, Nat. Photon. **7**, 613 (2013).

[47] Y. Ma, H. Miao, B. Pang, M. Evans, C. Zhao, J. Harms, R. Schnabel, and Y. Chen, Proposal for gravitational-wave detection beyond the standard quantum limit through EPR entanglement, Nat. Phys. **13**, 776 (2017).

[48] F. Y. Khalili and E. S. Polzik, Overcoming the standard quantum limit in gravitational wave detectors using spin systems with a negative effective mass, Phys. Rev. Lett. **121**, 031101 (2018).

[49] M. Tse, H. Yu, N. Kijbunchoo, A. Fernandez-Galiana, P. Dupej, L. Barsotti, C.D. Blair, D.D. Brown, S.E. Dwyer, A. Effler *et al.*, Quantum-enhanced advanced LIGO detectors in the era of gravitational-wave astronomy, Phys. Rev. Lett. **123**, 231107 (2019).

[50] Y. Zhao, N. Aritomi, E. Capocasa, M. Leonardi, M. Eisenmann, Y. Guo, E. Polini, A.Tomura, K. Arai, Y. Aso *et al.*, Frequency-dependent squeezed vacuum source for broadband quantum noise reduction in advanced gravitational-wave detectors, Phys. Rev. Lett. **124**, 171101 (2020).

[51] A. Kuzmich, K. Mølmer, and E. S. Polzik, Spin squeezing in an ensemble of atoms illuminated with squeezed light, Phys. Rev. Lett. **79**, 4782 (1997).

[52] J. Hald, J. L. Sørensen, C. Schori, and E. S. Polzik, Spin squeezed atoms: A macroscopic entangled ensemble created by light, Phys. Rev. Lett. **83**, 1319 (1999).

[53] L. Vernac, M. Pinard, and E. Giacobino, Spin squeezing in two-level systems, Phys. Rev. A **62**, 063812 (2000).

[54] M. Fleischhauer and S. Gong, Stationary source of nonclassical or entangled atoms, Phys. Rev. Lett. **88**, 070404 (2002).

[55] A. Dantan, M. Pinard, V. Josse, N. Nayak, and P. R. Berman, Atomic spin squeezing in a Λ system, Phys. Rev. A **67**, 045801 (2003).

[56] A. Dantan and M. Pinard, Quantum-state transfer between fields and atoms in electromagnetically induced transparency, Phys. Rev. A **69**, 043810 (2004).

[57] O. Hosten, N. J. Engelsen, R. Krishnakumar, and M. A. Kasevich, Measurement noise 100 times lower than the quantum-projection limit using entangled atoms, Nature (London) **529**, 505 (2016).

[58] A. Kuzmich, L. Mandel, and N. P. Bigelow, Generation of spin squeezing via continuous quantum nondemolition measurement, Phys. Rev. Lett. **85**, 1594 (2000).

[59] Z. Chen, J. G. Bohnet, S. R. Sankar, J. Dai, and J. K. Thompson, Conditional spin squeezing of a large ensemble via the vacuum Rabi splitting, Phys. Rev. Lett. **106**, 133601 (2011).

[60] M. A. C. Rossi, F. Albarelli, D. Tamascelli, and M. G. Genoni, Noisy quantum metrology enhanced by continuous nondemolition measurement, Phys. Rev. Lett. **125**, 200505 (2020).

[61] M. Kritsotakis, J. A. Dunningham, and S. A. Haine, Spin squeezing of a Bose-Einstein condensate via a quantum nondemolition measurement for quantum-enhanced atom interferometry, Phys. Rev. A **103**, 023318 (2021).

[62] E. O. Ilo-Okeke, S. Sunami, C. J. Foot, and T. Byrnes, Faraday-imaging-induced squeezing of a double-well Bose-Einstein condensate, Phys. Rev. A **104**, 053324 (2021).

[63] E. O. Ilo-Okeke, M. Kondappan, P. Chen, Y. Mao, V. Ivannikov, and T. Byrnes, Hybrid approximation approach to the generation of atomic squeezing with quantum nondemolition measurements, Phys. Rev. A **107**, 052604 (2023).

[64] C. Gross, T. Zibold, E. Nicklas, J. Estève, and M. K. Oberthaler, Nonlinear atom interferometer surpasses classical precision limit, Nature (London) **464**, 1165 (2010).

[65] M. F. Riedel, P. Böhi, Y. Li, T. W. Hänsch Signnsch, A. Sinatra, and P. Treutlein, Atom-chip-based generation of entanglement for quantum metrology, Nature (London) **464**, 1170 (2010).

[66] A. Sørensen, L.-M. Duan, J. I. Cirac, and P. Zoller, Many-particle entanglement with Bose-Einstein condensates, Nature (London) **409**, 63 (2001).

[67] C. Orzel, A. K. Tuchman, M. L. Fenselau, M. Yasuda, and M. A. Kasevich, Squeezed states in a Bose-Einstein condensate, Science **291**, 2386 (2001).

[68] M. Fadel, T. Zibold, B. Dccamps, and P. Treutlein, Spatial entanglement patterns and Einstein-Podolsky-Rosen steering in Bose-Einstein condensates, Science **360**, 409 (2018).

[69] G. S. Agarwal, R. R. Puri, and R. P. Singh, Atomic Schrödinger cat states, Phys. Rev. A **56**, 2249 (1997).

[70] A. Sondberg Sørensen and K. Mølmer, Entangling atoms in bad cavities, Phys. Rev. A **66**, 022314 (2002).

[71] J. Borregaard, E. J. Davis, G. S. Bentsen, M. H. Schleier-Smith, and A. S. Sørensen, One- and two-axis squeezing of atomic ensembles in optical cavities, New J. Phys. **19**, 093021 (2017).

[72] R. N. Deb, M. S. Sebawe Abdalla, S. S. Hassan, and N. Nayak, Spin squeezing and entanglement in a dispersive cavity, Phys. Rev. A **73**, 053817 (2006).

[73] E. G. Dalla Torre, J. Otterbach, E. Demler, V. Vuletic, and M. D. Lukin, Dissipative preparation of spin squeezed atomic ensembles in a steady state, Phys. Rev. Lett. **110**, 120402 (2013).

[74] Y. C. Zhang, X. F. Zhou, X. Zhou, G. C. Guo, and Z. W. Zhou, Cavity-assisted single-mode and two-mode spin-squeezed states via phase-locked atom-photon coupling, Phys. Rev. Lett. **118**, 083604 (2017).

[75] J. Hu, W. Chen, Z. Vendeiro, A. Urvoy, B. Braverman, and V. Vuletić, Vacuum spin squeezing, Phys. Rev. A **96**, 050301(R) (2017).

[76] Y. C. Liu, Z. F. Xu, G. R. Jin, and L. You, Spin squeezing: Transforming one-axis twisting into two-axis twisting, Phys. Rev. Lett. **107**, 013601 (2011).

[77] G. Liu, Y. N. Wang, L. F. Yan, N. Q. Jiang, W. Xiong, and M. F. Wang, Spin squeezing via one- and two-axis twisting induced by a single off-resonance stimulated Raman scattering in a cavity, Phys. Rev. A **99**, 043840 (2019).

[78] W. Qin, Y. H. Chen, X. Wang, A. Miranowicz and F. Nori, Strong spin squeezing induced by weak squeezing of light inside a cavity, Nanophotonics **9**, 4853 (2020).

[79] P. Groszkowski, H. K. Lau, C. Leroux, L. C. G. Govia, and A. A. Clerk, Heisenberg-limited spin squeezing via bosonic parametric driving, Phys. Rev. Lett. **125**, 203601 (2020).

[80] S. Y. Bai and J. H. An, Generating stable spin squeezing by squeezed-reservoir engineering, Phys. Rev. Lett. **127**, 083602 (2021).

[81] Z. Zhang, L. Shao, W. Lu, Y. Su, Y. P. Wang, J. Liu, and X. Wang, Single-photon-triggered spin squeezing with decoherence reduction in optomechanics via phase matching, Phys. Rev. A **104**, 053517 (2021).

[82] Y. Liu, J. Song, W. Qin, Y. H. Chen, and Y. Xia, Generation of spin squeezing via a fully quantum degenerate parametric amplifier, Phys. Rev. A **107**, 023724 (2023).

[83] L. G. Huang, X. Zhang, Y. Wang, Z. Hua, Y. Tang, and Y. C. Liu, Heisenberg-limited spin squeezing in coupled spin systems, Phys. Rev. A **107**, 042613 (2023).

[84] Z. Hu, Q. Li, X. Zhang, L. G. Huang, H. B. Zhang, and Y. C. Liu, Spin squeezing with arbitrary quadratic collective-spin interactions, Phys. Rev. A **108**, 023722 (2023).

[85] S. D. Bennett, N. Y. Yao, J. Otterbach, P. Zoller, P. Rabl, and M. D. Lukin, Phonon-induced spin-spin interactions in diamond nanostructures: Application to spin squeezing, Phys. Rev. Lett. **110**, 156402 (2013).

[86] Y. H. Ma and X. F. Zhang, Steady-state spin squeezing generation in diamond nanostructures, Phys. Rev. B **89**, 144113 (2014).

[87] P. B. Li, Y. Zhou, W. B. Gao, and F. Nori, Enhancing spin-phonon and spin-spin interactions using linear resources in a hybrid quantum system, Phys. Rev. Lett. **125**, 153602 (2020).

[88] J. Q. Chen, Y. F. Qiao, X. L. Dong, X. L. Hei, and P. B. Li, Dissipation-assisted preparation of steady spin-squeezed states of SiV centers, Phys. Rev. A **103**, 013709 (2021).

[89] G. Wang, Z. Li, X. Qin, Z. Yang, X. Li, X. Wu, Y. Zhou, and Y. Chen, Photon-phonon entanglement and spin squeezing via dynamically strain-mediated Kerr nonlinearity in dressed nitrogen-vacancy centers, Opt. Laser Technol. **176**, 110984 (2024).

[90] D. F. V. James, Quantum computation with hot and cold ions: An assessment of proposed schemes, Fortschr. Phys. **48**, 823 (2000).

[91] M. O. Scully and M. S. Zubairy, *Quantum Optics* (Cambridge University Press, Cambridge, 1997).

[92] P. Meystre and M. Sargent, *Elements of Quantum Optics* (Springer, Berlin, 1990).

[93] D. F. Walls and G. J. Milburn, *Quantum Optics* (Springer, Berlin, 1994).

[94] E. X. DeJesus and C. Kaufman, Routh-Hurwitz criterion in the examination of eigenvalues of a system of nonlinear ordinary differential equations, Phys. Rev. A **35**, 5288 (1987).

[95] H. Krauter, C. A. Muschik, K. Jensen, W. Wasilewski, J. M. Petersen, J. I. Cirac, and E. S. Polzik, Entanglement generated by dissipation and steady state entanglement of two macroscopic objects, Phys. Rev. Lett. **107**, 080503 (2011).

[96] D. F. Phillips, A. Fleischhauer, A. Mair, R. L. Walsworth, and M. D. Lukin, Storage of light in atomic vapor, Phys. Rev. Lett. **86**, 783 (2001).